Wang *et al.*
Chinese Journal of Mechanical Engineering (2022) 35:119
https://doi.org/10.1186/s10033-022-00781-6

Chinese Journal of Mechanical Engineering

ORIGINAL ARTICLE

Open Access

Inverse Dynamics of A 3-DOF Parallel Mechanism Based on Analytical Forward Kinematics

Ke Wang[1†], Ju Li[1*†], Huiping Shen[1], Jingjing You[2] and Tingli Yang[1]

Abstract

For the development of a parallel mechanism (PM), it is necessary to establish a dynamic model which can accurately meet the requirements of real-time control. Compared with the general dynamic analysis model based on the inverse kinematics, the dynamic analysis model based on the forward kinematics has the advantage of low-complexity. In this paper, a new type of 3-DOF PM with analytical forward displacement analysis is proposed. Different from the general dynamic analysis based on the inverse kinematics, the displacement, velocity and acceleration equations of the PM are established and solved by forward kinematics. The inverse dynamic equation of the PM is constructed and solved by analyzing the forces on each link and based on Newton-Euler method. Then the theoretical results of an example are compared with the simulation results, which shows that the simulation results are basically consistent with the theoretical results. And the maximum error of the driving force of each pair is 1.32%, 5.8% and 5.2%, respectively, which verifies the correctness of the dynamic model. The PM has a potential application prospect in the grasping, spraying and picking of workpieces. The research results of this paper provide a theoretical basis for the design, manufacture and application of the PM.

Keywords: Parallel mechanism, Dynamic model, Newton-Euler method, Simulation verification

1 Introduction

Compared with the series mechanism, the parallel mechanism (PM) has the advantages of compact structure, high rigidity and motion accuracy, etc. The topic has attracted extensive attention from the academic and industrial community for many years [1–6]. At present, research on PMs mainly focuses on the topology, kinematics, dynamics and control [7–12]. The dynamic analysis mainly studies the relationship between the input forces and the output forces. This is the determination of the maximum load carrying capacity and reasonable design of the driver during the development of parallel robots. According to this, the constraint reaction force of the motion pair solved during the analysis process plays an important role in the design, mechanical efficiency estimation, friction calculation, and mechanical vibration research of the various parts of the PM [13–17]. Therefore, for a PM to be developed, it is necessary to establish a dynamic model that can accurately meet the requirements of real-time control.

In terms of modeling methods, the commonly used dynamic modeling methods are Lagrangian method, universal equations of dynamics, Newton-Euler method, virtual work principle, Hamilton principle, Kane equation, etc. [18–23]. Among them, the universal equations of dynamics and Lagrange method are based on the system's virtual displacement and kinetic and potential energy respectively to build a simple dynamic model. While the Newton-Euler method can obtain the force of each joint by analyzing each member separately, and then

†Ke Wang and Ju Li are Co-first authors

*Correspondence: wangju0209@163.com

[1] Research Center for Advanced Mechanism Theory, Changzhou University, Changzhou 213016, China
Full list of author information is available at the end of the article

establishes a complete dynamic model by eliminating the interaction force of each member, it can also solve the support force and moment of force between members.

In terms of research objects, most of the dynamic analysis mainly focus on the 6-DOF Stewart PM [24, 25]. For 5-DOF PM, Chen et al. use the universal equations of dynamics to analyze the 4-UPS-UPU PM [26]. Li et al. used the Newton-Euler method to analyze the dynamics of the 5-PSS/UPU PM [23]. For 4-DOF PM, Geng used Newton-Euler to analyze the 4UPS-UPR PM [27]. In terms of 3-DOF, Li et al. used the Newton-Euler method to analyze the dynamics of a 3-RPS PM [28]. Liu et al. performed a Lagrangian method to analyze the dynamics of a 3-RRS PM [29].

In this paper, a 3-DOF 2T1R PM [30] with a forward analytical position solution is proposed. Firstly, the kinematics of the PM is analyzed. Then, force analysis is carried out for each component, and the dynamic model is established by Newton-Euler method. Finally, the correctness of the modeling method is verified by comparing the results of MATLAB calculation and ADAMS simulation. When the three prismatic pairs of the PM move at different speeds, it can undergo two-translation and one-rotation in a small range, while the three prismatic pairs move at the same speed, it can undergo one-translation DOF along the direction of the guide rail in a large range. Therefore, the PM has a potential application prospect in the grasping, spraying and picking of workpieces. The research results of this paper provide a theoretical basis for the design, manufacture and application of the PM.

2 Mechanism Architecture

The PM shown in Figure 1 consists of a moving platform, a base, and a complex branch chain and an unconstrained branch PSS (Prismatic pair - Spherical joint - Spherical joint) connecting the moving platform and the base. The sub-PM and an revolute pair are connected in series, where the two branches of the sub-PM are SOC_1 {-P⊥$P^{(4R)}$-}, SOC_2 {-P⊥R||R}, where $P^{(4R)}$ indicates that a parallelogram composed of 4 revolute pairs that is equivalent to a prismatic pair P, while SOC means single-open-chain that consists of link and pair in serial way. This PM can generate two translations in the Y and Z directions and a rotation output about the Y axis. The PM is referred to as the 2T1R PM [30].

2.1 Kinematics Analysis

The coordinate system shown in Figure 2 is established. The base coordinate system O-XYZ is established with the origin at the center point O of the guide rail where the driving pair A_1, A_2 is located, the positive half of the Y-axis is from O to A_2, and the positive half of the Z-axis is vertical upward. The moving coordinate system o-xyz is established with the origin at o point that is the center point O of the line $C_{12}C_2$ on the sub-moving platform. The positive half of the y-axis is from the origin o to C_2, and the z-axis is perpendicular to the plane of the moving platform.While the X and x axis direction meet the right-hand screw rule, the geometry parameters of each component are shown in Figure 2.

Establish the local coordinate system of each link B_iC_i (i=1, 2, 3). The x_1 axis of the coordinate system B_1-$x_1y_1z_1$ is parallel to the X axis of the base coordinate system, and the positive half of the z_1 axis is pointed from B_1 to C_1; The x_2 axis of the coordinate system B_2-$x_2y_2z_2$ is parallel to the X axis of the base coordinate system, and the positive half of the z_2 axis is pointed from B_2 to C_2, where the y axis of each coordinate system meets the right-hand screw rule; The positive half of the z_3 axis of the coordinate system B_3-$x_3y_3z_3$ is pointed from B_3 to C_3, and the x_3

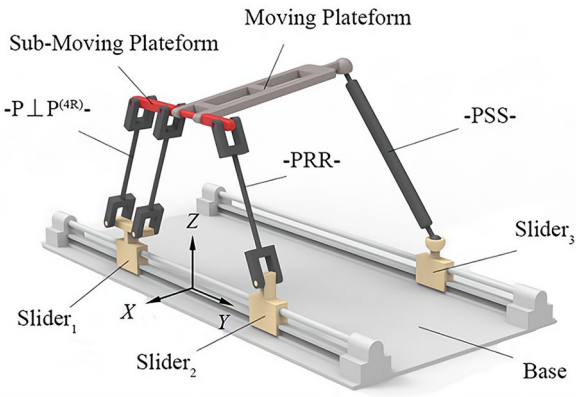

Figure 1 3D model of the 2T1R PM

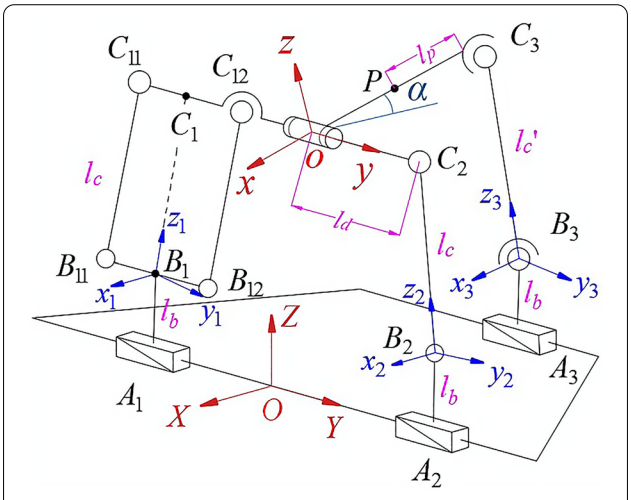

Figure 2 Schematic diagram of 2T1R PM

axis lies in the *XOZ* plane and the angle with the *X* axis is θ_1, its Euler transformation relative to the base coordinate system is shown in Figure 3, from which the coordinate transformation matrix from the coordinate system $\{B_3\}$ to the base coordinate system *O-XYZ* is:

$$^{O}\boldsymbol{R}_{l_3} = \boldsymbol{R}(Y,\theta_1)\boldsymbol{R}\left(x_3',\theta_2\right) .$$

2.2 Forward Position Solution

The forward kinematics of PM is to solve the position and orientation of the moving platform when the structural parameters and input of the mechanism are given.

Based on the constrained length of the bars, we can get:

$$\begin{cases} l_c^2-(z-l_b)^2-(y-l_d-l_1)^2=0, \\ l_c^2-(z-l_b)^2-(l_2-y-l_d)^2=0, \\ (-2l_p\cos\alpha-x_{A_3})^2+(y-l_3)^2+(z+2l_p\sin\alpha-l_b)^2=l_c'^2. \end{cases} \tag{1}$$

From Eq. (1), the coordinates of point *o* are:

$$\begin{aligned} y &= \frac{l_1+l_2}{2}, \\ z &= \sqrt{l_c^2-\left(\frac{l_2-l_1}{2}-l_d\right)^2}+l_b. \end{aligned} \tag{2}$$

Angle α of moving platform is:

$$\alpha = 2\arctan\left(\frac{-B\pm\sqrt{B^2-C^2+A^2}}{C-A}\right), \tag{3}$$

where

$$\begin{aligned} A &= 4(z-l_b)\cdot l_p, \\ B &= 4x_{A_3}\cdot l_p, \\ C &= -4l_p^2-x_{A_3}^2-\left(y-l_3\right)^2-(z-l_b)^2+l_c'^2. \end{aligned}$$

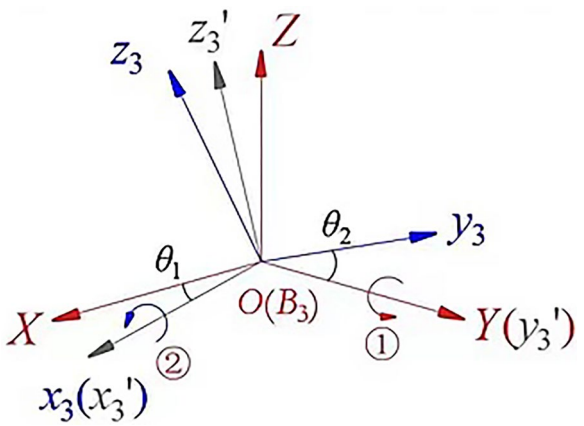

Figure 3 Coordinate system B_3-$x_3y_3z_3$ Euler transform

2.3 Velocity and Acceleration Analysis

2.3.1 Velocity and Acceleration of the Moving Platform

Taking the time derivative of Eqs. (2), (3), the output velocity and acceleration of the moving platform can be obtained as

$$\boldsymbol{\chi} = \left[\dot{y}\ \dot{z}\ \dot{\alpha}\right]^{\mathrm{T}}, \tag{4}$$

$$\dot{\chi} = \left[\ddot{y}\ \ddot{z}\ \ddot{\alpha}\right]^{\mathrm{T}}. \tag{5}$$

2.3.2 Velocity and Acceleration of Members

(1) Velocity and acceleration of member B_1C_1

Because the movements of the $B_{11}C_{11}$ and $B_{12}C_{12}$ rods are the same, the two rods are equivalent to the rod B_1C_1 for analysis.

The velocity of the point C_1 is:

$$\boldsymbol{v}_{c_1} = \boldsymbol{v}_o = \boldsymbol{v}_1 + \boldsymbol{\omega}_{l_1}\times\boldsymbol{c}_1\cdot l_c \tag{6}$$

where $\boldsymbol{v}_o$ is the linear velocity of point *o*;$\boldsymbol{v}_1$ is the linear velocity of the driving pair A_1;$\boldsymbol{c}_1$ and $\boldsymbol{\omega}_{l_1}$ are respectively the linear and angular velocity of the rod B_1C_1.

The angular velocity of the rod B_1C_1 can be determined by taking the cross product of the two sides of Eq. (6) with $\boldsymbol{c}_1$, which yields:

$$\boldsymbol{\omega}_{l_1} = \frac{\boldsymbol{c}_1\times\left(\boldsymbol{v}_{c_1}-\boldsymbol{v}_1\right)}{l_c}. \tag{7}$$

Substituting Eq. (7) into Eq. (8) to obtain the velocity of the center of mass of the rod B_1C_1,

$$\boldsymbol{v}_{l_1} = \boldsymbol{v}_1 + \boldsymbol{\omega}_{l_1}\times\boldsymbol{c}_1\cdot\frac{l_c}{2}. \tag{8}$$

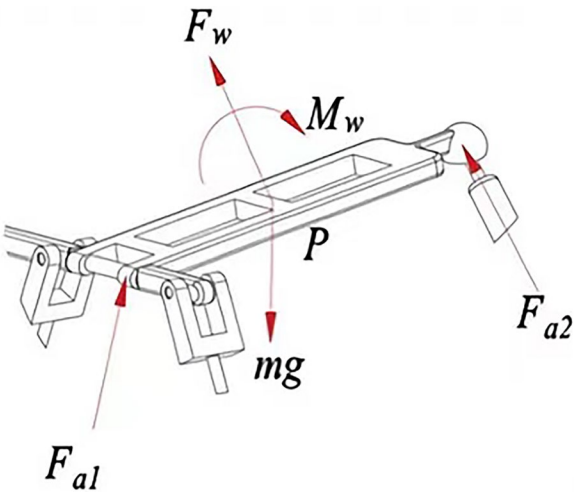

Figure 4 Force analysis of the moving platform

Taking the time derivative of Eq. (6), the acceleration of the C_1 can be obtained as:

$$\boldsymbol{a}_{c_1} = \boldsymbol{a}_o = \boldsymbol{a}_1 + \boldsymbol{\varepsilon}_{l_1} \times \boldsymbol{c}_1 \cdot l_c + \boldsymbol{\omega}_{l_1} \times \left(\boldsymbol{\omega}_{l_1} \times \boldsymbol{c}_1\right) \cdot l_c. \tag{9}$$

The angular acceleration of the rod B_1C_1 can be determined by taking the cross product of the two sides of Eq. (9) with $\boldsymbol{c}_1$, which yields:

$$\boldsymbol{\varepsilon}_{l_1} = \frac{\boldsymbol{c}_1 \times (\boldsymbol{a}_o - \boldsymbol{a}_1)}{l_c} = \frac{\tilde{\boldsymbol{c}}_1 \cdot (\boldsymbol{a}_o - \boldsymbol{a}_1)}{l_c}, \tag{10}$$

where $\tilde{\boldsymbol{c}}_1$ is the skew symmetric matrix associated with the vector $\boldsymbol{c}_1$.

Taking the time derivative of Eq. (6), the centroid acceleration of rod B_1C_1 can be obtained as:

$$\boldsymbol{a}_{l_1} = \boldsymbol{a}_1 + \boldsymbol{\varepsilon}_{l_1} \times \boldsymbol{c}_1 \cdot \frac{l_c}{2} + \boldsymbol{\omega}_{l_1} \times \frac{l_c}{2}\left(\boldsymbol{\omega}_{l_1} \times \boldsymbol{c}_1\right) = \frac{1}{2}(\boldsymbol{a}_1 + \boldsymbol{a}_o). \tag{11}$$

(2) Velocity and acceleration of member B_2C_2

Similarly, using the same method as the velocity and acceleration of the rod B_1C_1, the angular velocity of the rod B_2C_2 can be obtained as:

$$\boldsymbol{\omega}_{l_2} = \frac{\boldsymbol{c}_2 \times \left(\boldsymbol{v}_{c_2} - \boldsymbol{v}_2\right)}{l_c}. \tag{12}$$

The centroid velocity of the rod B_2C_2:

$$\boldsymbol{v}_{l_2} = \boldsymbol{v}_2 + \boldsymbol{\omega}_{l_2} \times \boldsymbol{c}_2 \cdot \frac{l_c}{2}. \tag{13}$$

Angular acceleration of rod B_2C_2:

$$\boldsymbol{\varepsilon}_{l_2} = \frac{\boldsymbol{c}_2 \times (\boldsymbol{a}_o - \boldsymbol{a}_2)}{l_c} = \frac{\tilde{\boldsymbol{c}}_2 \cdot (\boldsymbol{a}_o - \boldsymbol{a}_2)}{l_c}. \tag{14}$$

Centroid acceleration of rod B_2C_2:

$$\boldsymbol{a}_{l_2} = \boldsymbol{a}_2 + \boldsymbol{\varepsilon}_{l_2} \times \boldsymbol{c}_2 \cdot \frac{l_c}{2} + \boldsymbol{\omega}_{l_2} \times \frac{l_c}{2}\left(\boldsymbol{\omega}_{l_2} \times \boldsymbol{c}_2\right) = \frac{1}{2}(\boldsymbol{a}_2 + \boldsymbol{a}_o). \tag{15}$$

(3) Velocity and acceleration of rod B_3C_3

The velocity of the point C_3 is

$$\boldsymbol{v}_{c_3} = \boldsymbol{v}_o + \boldsymbol{\omega}_o \times \boldsymbol{c}_p = \boldsymbol{v}_3 + \boldsymbol{\omega}_{l_3} \times \boldsymbol{c}_3 \cdot \boldsymbol{l}'_{\mathbf{c}}. \tag{16}$$

The angular velocity of the rod B_3C_3 can be determined by taking the cross product of the two sides of Eq. (16) with $\boldsymbol{c}_3$, which yields:

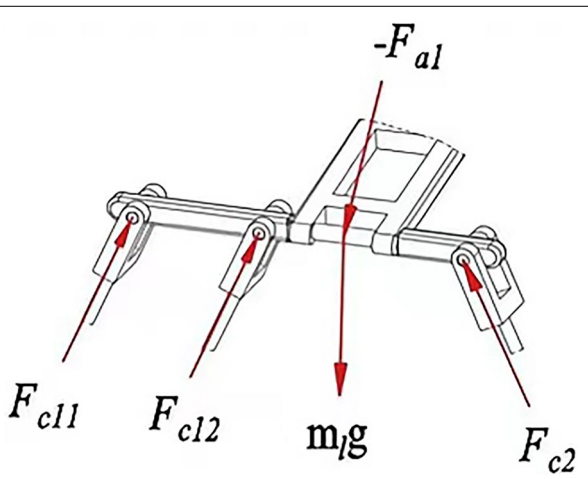

Figure 5 Force analysis of sub-moving platform

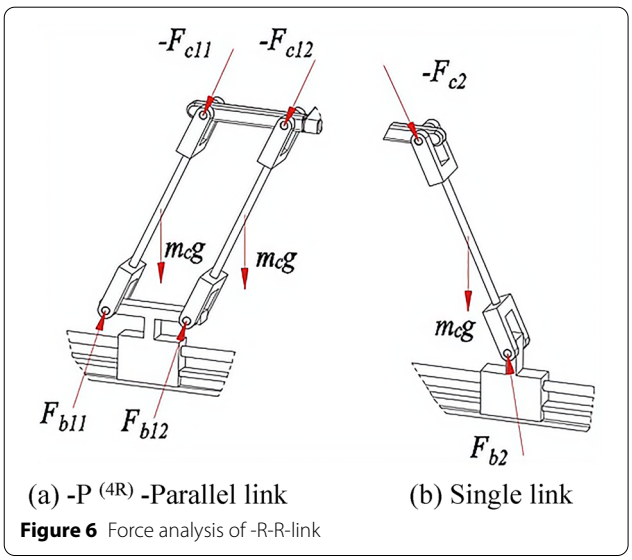

Figure 6 Force analysis of -R-R-link

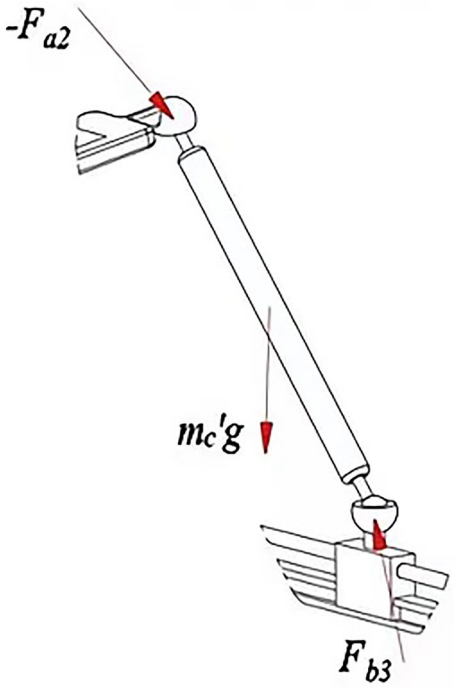

Figure 7 Force analysis diagram of -S-S- Link

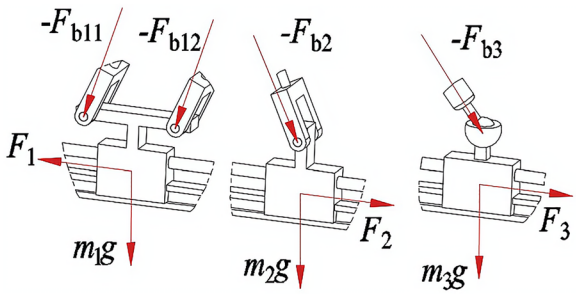

(a) Slider 1 (A_1) (b) Slider 2 (A_2) (c) Slider 3 (A_3)

Figure 8 Force analysis of three drive sliders

$$\boldsymbol{\omega}_{l_3} = \frac{\boldsymbol{c}_3 \times (\boldsymbol{v}_{c_3} - \boldsymbol{v}_3)}{l_c'}. \tag{17}$$

Substituting Eq. (17) into Eq. (18) gives the velocity at the centroid of rod B_3C_3:

$$\boldsymbol{v}_{l_3} = \boldsymbol{v}_3 + \boldsymbol{\omega}_{l_3} \times \boldsymbol{c}_3 \cdot \frac{l_c'}{2}. \tag{18}$$

Taking the time derivative of Eq. (16) , the acceleration of the $\boldsymbol{c}_3$ can be obtained as:

$$\begin{aligned} \boldsymbol{a}_{c_3} &= \boldsymbol{a}_o + \boldsymbol{\varepsilon}_o \times \boldsymbol{c}_p + \boldsymbol{\omega}_o \times (\boldsymbol{\omega}_o \times \boldsymbol{c}_p) \\ &= \boldsymbol{a}_3 + \boldsymbol{\varepsilon}_{l_3} \times \boldsymbol{c}_3 \cdot l_c' + \boldsymbol{\omega}_{l_3} \times (\boldsymbol{\omega}_{l_3} \times \boldsymbol{c}_3) l_c'. \end{aligned} \tag{19}$$

The angular acceleration of the rod B_3C_3 can be determined by taking the cross product of the two sides of Eq. (19) with $\boldsymbol{c}_3$,which yields:

$$\boldsymbol{\varepsilon}_{l_3} = \frac{\boldsymbol{c}_3 \times (\boldsymbol{a}_{c_3} - \boldsymbol{a}_3)}{l_c'} = \frac{\tilde{\boldsymbol{c}}_3 \cdot (\boldsymbol{a}_{c_3} - \boldsymbol{a}_3)}{l_c'}. \tag{20}$$

Taking the time derivative of Eq. (18) , the acceleration of the centroid of B_3C_3 can be obtained as:

$$\boldsymbol{a}_{l_3} = \boldsymbol{a}_3 + \boldsymbol{\varepsilon}_{l_3} \times \boldsymbol{c}_3 \cdot \frac{l_c'}{2} + \boldsymbol{\omega}_{l_3} \times \frac{l_c'}{2}(\boldsymbol{\omega}_{l_3} \times \boldsymbol{c}_3) = \frac{1}{2}(\boldsymbol{a}_3 + \boldsymbol{a}_{c_3}) . \tag{21}$$

3 Dynamics Modeling of Mechanism

When using the Newton-Euler method, the friction of each moving pair is not considered, then the Newton-Euler equation of each member is established. Then the dynamic model of the PM is obtained by eliminating the internal forces between the members. Finally, the relationship between the driving force and the external forces of the moving platform is obtained, which is illustrated as follows.

3.1 Dynamic Equation of Moving Platform

As shown in Figure 4, the gravity of the moving platform is $\boldsymbol{mg}$, the constraint force of the sub-moving platform is $\boldsymbol{F}_{a1}$, and the constraint force of the PSS branch chain is $\boldsymbol{F}_{a2}$. The external force and moment of the moving platform are $\boldsymbol{F}_w$ and $\boldsymbol{M}_w$ respectively.

The dynamic equation of the moving platform is:

$$\boldsymbol{F}_w + \boldsymbol{F}_{a1} + \boldsymbol{F}_{a2} + m\boldsymbol{g} = m\boldsymbol{a}_p, \tag{22}$$

$$\boldsymbol{M}_w - \frac{1}{2}\boldsymbol{c}_p \times \boldsymbol{F}_{a1} + \frac{1}{2}\boldsymbol{c}_p \times \boldsymbol{F}_{a2} = {}^o\boldsymbol{I}_p\boldsymbol{\varepsilon}_p + \boldsymbol{\omega}_p \times ({}^o\boldsymbol{I}_p\boldsymbol{\omega}_p) , \tag{23}$$

where ${}^o\boldsymbol{I}_p = {}^o\boldsymbol{R}_p\boldsymbol{I}_p{}^o\boldsymbol{R}_p^{\mathrm{T}}$; ${}^o\boldsymbol{R}_p$ is the transformation matrix of the moving coordinate system to the base coordinate system;${}^o\boldsymbol{I}_p$ is the inertia tensor of the moving platform in the base frame;$\boldsymbol{I}_p$ is the inertia tensor of the moving platform in the local frame;$\boldsymbol{c}_p$ is the position vector from the center of mass of the moving platform to the center of the spherical joint on the moving platform.

3.2 Dynamic Equation of the Sub-Moving Platform

As shown in Figure 5, the dynamic equation of the sub-moving platform can be written as follows:

$$-\boldsymbol{F}_{a1} + m_l\boldsymbol{g} + \boldsymbol{F}_{c11} + \boldsymbol{F}_{c12} + \boldsymbol{F}_{c2} = m_l\boldsymbol{a}_o. \tag{24}$$

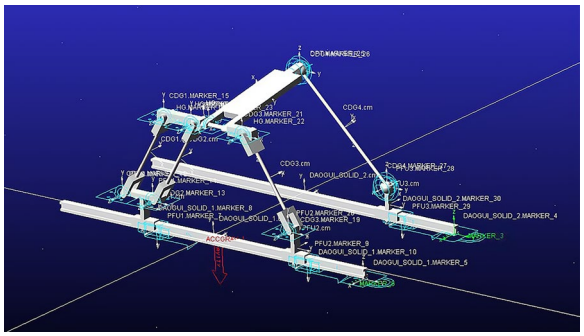

Figure 9 Virtual prototype of 2T1R parallel mechanism

where $\boldsymbol{F_{c11}}$, $\boldsymbol{F_{c12}}$, $\boldsymbol{F_{c2}}$ are constraint forces of the active link B_iC_i (i=1,2)in the sub-moving platform; m_l is mass of the sub-moving platform; $-\boldsymbol{F_{a1}}$ is the reaction force of the moving platform.

3.3 Dynamic Equation of Connecting Rod

The R-R-link is subject to the constraint reaction force of the sub-moving platform $-\boldsymbol{F}_{ci}$ (i=1, 2), its own gravity $m_c\boldsymbol{g}$, and the constraint force $\boldsymbol{F}_{bi}$ (i = 1, 2), and its force analysis is shown in Figure 6.

Therefore, the dynamic equations of the two parallel links in the parallelogram are as follows:

$$-\boldsymbol{F}_{c1i} + m_c\boldsymbol{g} + \boldsymbol{F}_{b1i} = m_c\boldsymbol{a}_{li},\ (i = 1, 2), \tag{25}$$

$$\frac{l_c}{2}\boldsymbol{c}_i \times (-\boldsymbol{F}_{ci}) + \frac{l_c}{2}(-\boldsymbol{c}_i) \times \boldsymbol{F}_{bi} = {}^o\boldsymbol{I}_{li}\boldsymbol{\varepsilon}_{li} + \boldsymbol{\omega}_{li} \times \left({}^o\boldsymbol{I}_{li}\boldsymbol{\omega}_{li}\right). \tag{26}$$

Dynamic equation of single link (B_2C_2) is as follows:

$$-\boldsymbol{F}_{c2} + m_c\boldsymbol{g} + \boldsymbol{F}_{b2} = m_c\boldsymbol{a}_{l2}, \tag{27}$$

$$\frac{l_c}{2}\boldsymbol{c}_2 \times (-\boldsymbol{F}_{c2}) + \frac{l_c}{2}(-\boldsymbol{c}_2) \times \boldsymbol{F}_{b2} = {}^o\boldsymbol{I}_{l2}\boldsymbol{\varepsilon}_{l2} + \boldsymbol{\omega}_{l2} \times \left({}^o\boldsymbol{I}_{l2}\boldsymbol{\omega}_{l2}\right), \tag{28}$$

where ${}^o\boldsymbol{I}_{li} = {}^o\boldsymbol{R}_{li}\boldsymbol{I}_{li}{}^o\boldsymbol{R}_{li}^{\mathrm{T}}$, ($i$ = 1, 2),${}^o\boldsymbol{I}_{li}$ is the inertia tensor of the connecting rod in the base frame ;$\boldsymbol{I}_{li}$ is the inertia tensor of the connecting rod in the local frame;${}^o\boldsymbol{R}_{li}$ is the transformation matrix from the local frames of the connecting rod to the base frame.

Further, -*S*-*S*-link (B_3C_3) is subject to the constraint reaction force of the moving platform$-\boldsymbol{F}_{a2}$, the constraint force of the drive member $\boldsymbol{F}_{b3}$, the self-gravity m_c'g, while m_c' is the mass of -*S*-*S*- connecting rod, and its stress is shown in Figure 7.

Table 1 Dimension Parameters of the 2T1R PM

Size parameter	Value
l_b (mm)	10
l_d (mm)	17
l_c (mm)	43.8
l_c' (mm)	60
$-XA_3$ (mm)	60
$2lp$ (mm)	54
m_1 (kg)	0.00254
m_2 (kg)	0.00162
m_3 (kg)	0.00153
m_c (kg)	0.00285
m_c' (kg)	0.00129
m_l (kg)	0.00491
m (kg)	0.0131

Then, the dynamic equations of the -S-S- link are described as

$$-\boldsymbol{F}_{\mathrm{a2}} + m_c'\boldsymbol{g} + \boldsymbol{F}_{b3} = m_c'\boldsymbol{a}_{l3}, \tag{29}$$

$$\frac{l_c'}{2}\boldsymbol{c}_3 \times (-\boldsymbol{F}_{a2}) + \frac{l_c'}{2}(-\boldsymbol{c}_3) \times \boldsymbol{F}_{b3} = {}^o\boldsymbol{I}_{l3}\boldsymbol{\varepsilon}_{l3} + \boldsymbol{\omega}_{l3} \times \left({}^o\boldsymbol{I}_{l3}\boldsymbol{\omega}_{l3}\right), \tag{30}$$

where ${}^o\boldsymbol{I}_{l3} = {}^o\boldsymbol{R}_{l3}\boldsymbol{I}_{l3}{}^o\boldsymbol{R}_{l3}^{\mathrm{T}}$.

3.4 Dynamic Equation of Driving Sliders

The three driving sliders are subject to the constraint reaction forces of each link $-F_{bi}$ (i = 1, 2, 3), its own gravity, and the driving force of the driving motor $m_i\boldsymbol{g}$ (i = 1,2, 3), and the force diagram of the slider is shown in Figure 8.

The dynamic equation of slider 1 is

$$\boldsymbol{F}_1 - \boldsymbol{F}_{b11} - \boldsymbol{F}_{b12} + m_1\boldsymbol{g} = m_1\boldsymbol{a}_1. \tag{31}$$

The dynamic equations of slider 2 and slide 3 are as follows:

$$\boldsymbol{F}_i - \boldsymbol{F}_{bi} + m_i\boldsymbol{g} = m_i\boldsymbol{a}_i.\ (i = 2, 3) \tag{32}$$

3.5 The Integrated Dynamic Model of the PM

The establishment of the integrated dynamic model is to eliminate the internal forces of members and to obtain the dynamic relationship between the input force, torque and output force.

Taking the dot product of the both sides of Eq. (31) with $\boldsymbol{e}_1^{\mathrm{T}}$

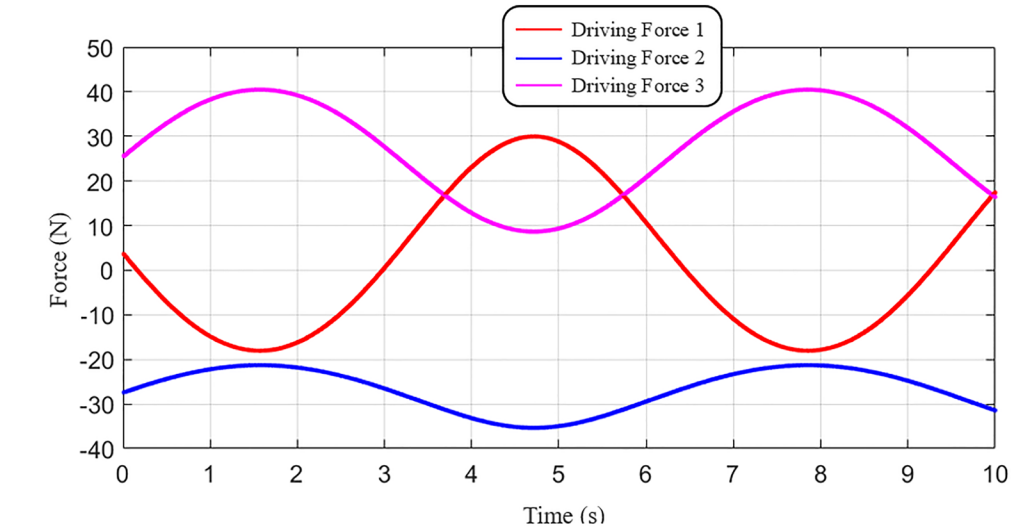

(a) Theoretical driving force

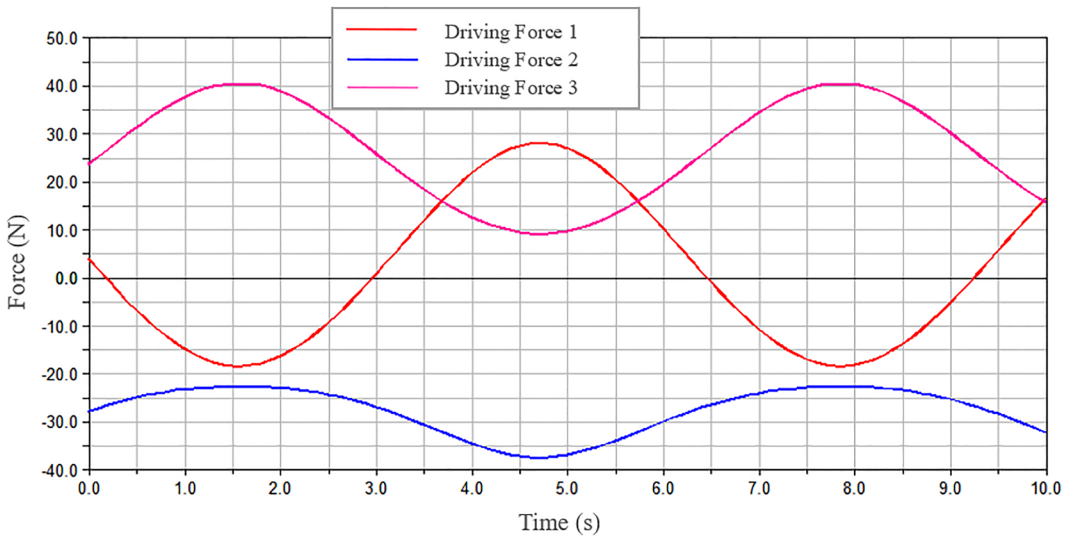

(b) Driving force simulation value

Figure 10 Driving force of each driving pair

$$\tau_1 = \boldsymbol{e}_1^{\mathrm{T}} \cdot \boldsymbol{F}_1 = \boldsymbol{e}_1^{\mathrm{T}} \cdot (\boldsymbol{F}_{b11} + \boldsymbol{F}_{b12}) + m_1 \boldsymbol{a}_1, \tag{33}$$

where $\tau_i (i = 1, 2, 3)$ is the driving force of the slider, $\boldsymbol{e}_i (i = 1, 2, 3)$ is the unit vector for driving force.

Substituting Eq. (25) into Eq. (33), we can write:

$$\tau_1 = \boldsymbol{e}_1^{\mathrm{T}} \cdot \sum_{i=1}^{2} (\boldsymbol{F}_{c1i} - m_c \boldsymbol{g} + m_c \boldsymbol{a}_{li}) + m_1 \boldsymbol{a}_1. \tag{34}$$

Table 2 Matlab calculation time

Simulation duration (s)	Step size (s)	Calculation time (s)
10	0.01	4.77
10	0.005	9.13
10	0.004	11.64

According to Eq. (26),we can write:

$$l_c \boldsymbol{c}_1 \times \left(\boldsymbol{F}_{c_{11}} + \boldsymbol{F}_{c_{12}}\right) = \boldsymbol{C}_1, \tag{35}$$

$$\boldsymbol{C}_1 = l_c \boldsymbol{c}_1 \times (m_c \boldsymbol{g} - m_c \boldsymbol{a}_{l1}) - 2^o \boldsymbol{I}_{l1} \boldsymbol{\varepsilon}_{l1} - 2\boldsymbol{\omega}_{l1} \times \left({}^o \boldsymbol{I}_{l1} \boldsymbol{\omega}_{l1}\right). \tag{36}$$

Taking the cross product of the two sides of Eq. (35) with $\boldsymbol{e}_1$ gives:

$$l_c \boldsymbol{e}_1 \times \boldsymbol{c}_1 \times (\boldsymbol{F}_{c11} + \boldsymbol{F}_{c12}) = \boldsymbol{e}_1 \times \boldsymbol{C}_1. \tag{37}$$

Then, we can write:

$$\boldsymbol{F}_{c11} + \boldsymbol{F}_{c12} = \frac{\boldsymbol{c}_1 \left[\boldsymbol{e}_1^{\mathrm{T}} (\boldsymbol{F}_{c11} + \boldsymbol{F}_{c12})\right]}{\boldsymbol{e}_1^{\mathrm{T}} \cdot \boldsymbol{c}_1} - \frac{\boldsymbol{e}_1 \times \boldsymbol{C}_1}{l_c \boldsymbol{e}_1^{\mathrm{T}} \boldsymbol{c}_1}. \tag{38}$$

According to Eq. (34), we can get:

$$\boldsymbol{e}_1^{\mathrm{T}} (\boldsymbol{F}_{c11} + \boldsymbol{F}_{c12}) = \tau_1 + 2\boldsymbol{e}_1^{\mathrm{T}} (m_c \boldsymbol{g} - m_c \boldsymbol{a}_{l1}) - m_1 \boldsymbol{a}_1. \tag{39}$$

Substituting Eq. (39) into Eq. (38) gives:

$$\boldsymbol{F}_{c11} + \boldsymbol{F}_{c12} = \frac{\boldsymbol{c}_1 \left[\tau_1 + 2\boldsymbol{e}_1^{\mathrm{T}} (m_c \boldsymbol{g} - m_c \boldsymbol{a}_{l1}) - m_1 \boldsymbol{a}_1\right]}{\boldsymbol{e}_1^{\mathrm{T}} \cdot \boldsymbol{c}_1} - \frac{\boldsymbol{e}_1 \times \boldsymbol{C}_1}{l_c \boldsymbol{e}_1^{\mathrm{T}} \boldsymbol{c}_1}. \tag{40}$$

Similarly,

$$\boldsymbol{F}_{c2} = \frac{\boldsymbol{c}_2 \left[\tau_2 + \boldsymbol{e}_2^{\mathrm{T}} (m_c \boldsymbol{g} - m_c \boldsymbol{a}_{l2}) - m_2 \boldsymbol{a}_2\right]}{\boldsymbol{e}_2^{\mathrm{T}} \cdot \boldsymbol{c}_2} - \frac{\boldsymbol{e}_2 \times \boldsymbol{C}_2}{l_c \boldsymbol{e}_2^{\mathrm{T}} \boldsymbol{c}_2}, \tag{41}$$

$$\boldsymbol{F}_{a2} = \frac{\boldsymbol{c}_3 \left[\tau_3 + \boldsymbol{e}_3^{\mathrm{T}} (m_c' \boldsymbol{g} - m_c' \boldsymbol{a}_{l3}) - m_3 \boldsymbol{a}_3\right]}{\boldsymbol{e}_3^{\mathrm{T}} \cdot \boldsymbol{c}_3} - \frac{\boldsymbol{e}_3 \times \boldsymbol{C}_3}{l_c \boldsymbol{e}_3^{\mathrm{T}} \boldsymbol{c}_3}, \tag{42}$$

where

$$\boldsymbol{C}_2 = l_c \boldsymbol{c}_2 \times (m_c \boldsymbol{g} - m_c \boldsymbol{a}_{l2}) - {}^o \boldsymbol{I}_{l2} \boldsymbol{\varepsilon}_{l2} - \boldsymbol{\omega}_{l2} \times \left({}^o \boldsymbol{I}_{l2} \boldsymbol{\omega}_{l2}\right),$$

$$\boldsymbol{C}_3 = l_c' \boldsymbol{c}_3 \times \left(m_c' \boldsymbol{g} - m_c' \boldsymbol{a}_{l3}\right) - {}^o \boldsymbol{I}_{l3} \boldsymbol{\varepsilon}_{l3} - \boldsymbol{\omega}_{l3} \times \left({}^o \boldsymbol{I}_{l3} \boldsymbol{\omega}_{l3}\right).$$

Substituting Eqs. (40) and (41) into Eq. (24), we can get

$$\boldsymbol{F}_{a1} = m_l \boldsymbol{g} + \boldsymbol{F}_{c11} + \boldsymbol{F}_{c12} + \boldsymbol{F}_{c2} - m_l \boldsymbol{a}_o. \tag{43}$$

Substituting Eqs. (42) and (43) into Eq. (22) and Eq. (23), we have

$$\begin{bmatrix} \boldsymbol{D} \\ \boldsymbol{E} \end{bmatrix}_{6\times 1} = \boldsymbol{J}_\tau \cdot \boldsymbol{\tau} + \begin{bmatrix} \boldsymbol{F}_w \\ \boldsymbol{M}_w \end{bmatrix}_{6\times 1}, \tag{44}$$

where

$$\boldsymbol{D} = -\frac{\boldsymbol{c}_1 \left[2\boldsymbol{e}_1^{\mathrm{T}} (m_c \boldsymbol{g} - m_c \boldsymbol{a}_{l1}) - m_1 \boldsymbol{a}_1\right]}{\boldsymbol{e}_1^{\mathrm{T}} \boldsymbol{c}_1} - \frac{\boldsymbol{c}_2 \left[\boldsymbol{e}_2^{\mathrm{T}} (m_c \boldsymbol{g} - m_c \boldsymbol{a}_{l2}) - m_2 \boldsymbol{a}_2\right]}{\boldsymbol{e}_2^{\mathrm{T}} \boldsymbol{c}_2} + \sum_{i=1}^{2} \frac{\boldsymbol{e}_i \times \boldsymbol{C}_i}{l_c \boldsymbol{e}_i^{\mathrm{T}} \boldsymbol{c}_i} - \frac{\boldsymbol{c}_3 \left[\boldsymbol{e}_3^{\mathrm{T}} \left(m_c' \boldsymbol{g} - m_c' \boldsymbol{a}_{l3}\right) - m_3 \boldsymbol{a}_3\right]}{\boldsymbol{e}_3^{\mathrm{T}} \boldsymbol{c}_3} + \frac{\boldsymbol{e}_3 \times \boldsymbol{C}_3}{l_c' \boldsymbol{e}_3^{\mathrm{T}} \boldsymbol{c}_3} - m_l (\boldsymbol{g} - \boldsymbol{a}_o) - m\left(\boldsymbol{g} - \boldsymbol{a}_p\right),$$

$$\boldsymbol{E} = \frac{1}{2} \boldsymbol{c}_p \times \left[\frac{\boldsymbol{c}_1 \left[2\boldsymbol{e}_1^{\mathrm{T}} (m_c \boldsymbol{g} - m_c \boldsymbol{a}_{l1}) - m_1 \boldsymbol{a}_1\right]}{\boldsymbol{e}_1^{\mathrm{T}} \boldsymbol{c}_1} + \frac{\boldsymbol{c}_2 \left[\boldsymbol{e}_2^{\mathrm{T}} (m_c \boldsymbol{g} - m_c \boldsymbol{a}_{l2}) - m_2 \boldsymbol{a}_2\right]}{\boldsymbol{e}_2^{\mathrm{T}} \boldsymbol{c}_2} - \sum_{i=1}^{2} \frac{\boldsymbol{e}_i \times \boldsymbol{C}_i}{l_c \boldsymbol{e}_i^{\mathrm{T}} \boldsymbol{c}_i} + m_l (\boldsymbol{g} - \boldsymbol{a}_o)\right] - \frac{1}{2} \boldsymbol{c}_p \times \left[\frac{\boldsymbol{c}_3 \left[\boldsymbol{e}_3^{\mathrm{T}} \left(m_c' \boldsymbol{g} - m_c' \boldsymbol{a}_{l3}\right) - m_3 \boldsymbol{a}_3\right]}{\boldsymbol{e}_3^{\mathrm{T}} \boldsymbol{c}_3} - \frac{\boldsymbol{e}_3 \times \boldsymbol{C}_3}{l_c' \boldsymbol{e}_3^{\mathrm{T}} \boldsymbol{c}_3}\right] - {}^o \boldsymbol{I}_p \boldsymbol{\varepsilon}_p - \boldsymbol{\omega}_p \times \left({}^o \boldsymbol{I}_p \boldsymbol{\omega}_p\right),$$

$$\boldsymbol{J}_\tau = \begin{bmatrix} \frac{\boldsymbol{c}_1}{\boldsymbol{e}_1^{\mathrm{T}} \boldsymbol{c}_1} & \frac{\boldsymbol{c}_2}{\boldsymbol{e}_2^{\mathrm{T}} \boldsymbol{c}_2} & \frac{\boldsymbol{c}_3}{\boldsymbol{e}_3^{\mathrm{T}} \boldsymbol{c}_3} \\ -\frac{\boldsymbol{c}_p \times \boldsymbol{c}_1}{2\boldsymbol{e}_1^{\mathrm{T}} \boldsymbol{c}_1} & -\frac{\boldsymbol{c}_p \times \boldsymbol{c}_2}{2\boldsymbol{e}_2^{\mathrm{T}} \boldsymbol{c}_2} & \frac{\boldsymbol{c}_p \times \boldsymbol{c}_3}{2\boldsymbol{e}_3^{\mathrm{T}} \boldsymbol{c}_3} \end{bmatrix}_{6\times 3},$$

$$\boldsymbol{\tau} = \left[\begin{array}{ccc} \tau_1 & \tau_2 & \tau_3 \end{array}\right]^{\mathrm{T}}_{3\times 1}.$$

According to Eq. (44), we can get:

$$\boldsymbol{\tau} = \boldsymbol{J}_{\tau}^{-1} \cdot \left[\begin{array}{c} \boldsymbol{D} \\ \boldsymbol{E} \end{array}\right] - \boldsymbol{J}_{\tau}^{-1} \cdot \left[\begin{array}{c} \boldsymbol{F}_w \\ \boldsymbol{M}_w \end{array}\right]. \tag{45}$$

When the motion law of the moving platform and the external force and torque are known, the driving force of each driving pair can be obtained from Eq. (45).

4 Dynamic Simulation

Firstly, the following motion laws of three driving pairs are given:

$$\begin{cases} l_1 = 10\cos(t) - 27, \\ l_2 = -10\cos(t) + 27, \\ l_3 = -10\cos(t) + 14. \end{cases} \tag{46}$$

A three-dimensional prototype of the PM is designed, as shown in Figure 9. The dimension parameters of the PM are shown in Table 1.

The above parameters are substituted into the dynamic Eqs. (22)–(45), and the driving forces of the three driving pairs are calculated by MATLAB. The curves of the driving forces are shown in Figure 10(a).

Then, the three-dimensional prototype is input into ADAMS, and the material properties of each part and the constraint types of the kinematic pairs are specified. The vertical downward gravity is applied, and the simulation step of 0.01 s and the simulation time of 10 s are selected for dynamic simulation of the virtual prototype.

As shown in Figure 10(b), the calculated value is compared with the simulation result of ADAMS, which shows that the simulation value is basically consistent with the theoretical value. The maximum error of the driving force of each pair is 1.32%, 5.8% and 5.2%, which verifies the correctness of the dynamic model.

In the same simulation duration, different steps are selected to record the calculation time of MATLAB, as shown in Table 2.

As shown in Table 2, only when the step size $\leq$0.005 s, the dynamic modeling analysis program is real-time.

5 Conclusions

(1) A new type of 3-DOF PM is proposed in this paper, and its analytical solution of forward kinematics is given, which is used to analyze its velocity and acceleration.

(2) Based on Newton-Euler method, the dynamic model of the PM is established by the analysis of force on each component.

(3) The dynamic simulation of the three-dimensional prototype is carried out by ADAMS, and the simulation results are compared with the theoretical calculation results of the example. The results show that the simulation results are basically consistent with the theoretical results, which verifies the correctness of the dynamic model.

Authors' Contributions

JL was in charge of the paper; KW wrote the manuscript; HS conceived the parallel mechanism. JY suggested the method of dynamic analysis; TY discussed the structure of the paper. All authors read and approved the final manuscript.

Authors' Information

Ke Wang, born in 1994, is currently an engineer at *Black & Decker(Suzhou) Technology Limited Company, China*. He received his master degree from *Changzhou University, China*, in 2020.

Ju Li, born in 1981, is currently a vice professor at *Changzhou University, China*. Her main research interests include parallel mechanism, kinematics.

Huiping Shen, born in 1965, is currently a professor and a PhD candidate supervisor at *Changzhou University, China*. His main research interests include parallel mechanism, kinematics, topology.

Jingjing You, born in 1985, is currently a vice professor and a master supervisor at *College of Mechanical and Electronic Engineering, Nanjing Forestry University, China*.

Ting-li Yang, born in 1940, is currently a guest professor at *Changzhou University, China*. His main research interest include modern mechanisms, basic theory of robotic mechanisms.

Funding

Supported by National Natural Science Foundation of China (Grant Nos. 51975062, 51475050).

Competing Interests

The authors declare no competing financial interests.

Author Details

[1]Research Center for Advanced Mechanism Theory, Changzhou University, Changzhou 213016, China. [2]College of Mechanical and Electronic Engineering, Nanjing Forestry University, Nanjing 210042, China.

Received: 10 August 2020 Revised: 13 April 2021 Accepted: 11 July 2022
Published online: 09 September 2022

References

[1] S Briot, I A Bonev. Pantoptern-4: A new 3T1R decoupled parallel manipulator for pick-and-place application. *Mechanism and Machine Theory*, 2010, 45(5): 707-721.

[2] H P Shen, M Lv, X R Zhu, et al. Topological design and kinematics of a single-degree-of-freedom 3T1R parallel mechanism. *China Mechanical Engineering*, 2019, 30(8): 961-968.

[3] J M Deng, K Xu, Y C Zhao, et al. Design and kinematics analysis of asymmetric 2T1R-type spatial parallel mechanism without parasitic motion. *Transactions of the Chinese Society for Agricultural Machinery*, 2018, 49(6): 408-417.

[4] T L Yang, A X Liu, H P Shen, et al. *Topology design of robot mechanisms*. Singapore: Springer, 2018.

[5] B Y Chang, X N Li, G G Jin, et al. Kinematics analysis of a 3t1r parallel mechanism with full-circle rotation capability. *Journal of Agricultural Machinery*, 2019, 50(7): 406-416.

[6] G L Yan, C C Wu, Q Y Chen, et al. Kinematics analysis and design optimization of novel 3t1r parallel manipulator. *Transactions of the Chinese Society for Agricultural Machinery*, 2017, 48(12): 386-394, 420.
[7] S F Yang, T Sun, T Huang. Type synthesis of parallel mechanisms having 3T1R motion with variable rotational axis. *Mechanism and Machine Theory*, 2017, 109: 220-230.
[8] M Bennehar, A Chemori, F Pierrot. A new revised desired compensation adaptive control for enhanced tracking: application to RA-PKMs. *Advanced Robotics*, 2016, 30(17-18): 1192-1214.
[9] H P Shen, K Xu, T L Yang, et al. Design and kinematics of a new 3T1R parallel manipulator 2- (RPa3R) 3R with zero coupling and motion decoupling. *Journal of Mechanical Engineering*, 2019, 55(5): 53-64.
[10] W Liu, H Z Liu. Type synthesis of 3-DOF parallel mechanism with both 2R1T and 3R motion mode. *Journal of Mechanical Engineering*, 2019, 55(3): 53-63. (in Chinese)
[11] Z M Chen, X M Liu, Y Zha, et al. Dynamics analysis of a symmetrical 2R1T 3-UPU parallel mechanism. *Journal of Mechanical Engineering*, 2017, 53(21): 46-53. (in Chinese)
[12] X Y Wang, S Guo, H B Qu, et al. Optimal allocation method of parallel mechanism and its application. *Journal of Mechanical Engineering*, 2019, 55(1): 44-53. (in Chinese)
[13] Y L Xu, L Yang, Z Y Yang, et al. Dynamics property analysis of a novel PURU+RR+S spherical parallel humanoid robotic ankle mechanism. *China Mechanical Engineering*, 2017, 28(16): 1971-1976.
[14] J T Yao, B Han, Y C Dou, et al. Influence of base motion on dynamic performance of parallel adjustment mechanism. *Transactions of the Chinese Society for Agricultural Machinery*, 2018, 49(7): 410-418.
[15] X H Jia, Y L Tian, D W Zhang. Inverse dynamics of 3-RRPR compliant precision positioning stage based on the principle of virtue work. *Journal of Mechanical Engineering*, 2011, 47(1): 68- 74. (in Chinese)
[16] S T Liu, T Huang, J P Mei, et al. Optimal design of a 4-DOF SCARA type parallel robot using dynamic performance indices and angular constrains. *Journal of Mechanisms and Robotics*, 2012, 4(3): 031005.
[17] J B Zhou, J J You, J Li, et al. Inverse dynamic of 2T1R parallel mechanism with symbolic positive position solution. *Machine Design and Research*, 2020, 36(3): 23-29.
[18] H Kalani, A Rezaei, A Akbarzadeh. Improved general solution for the dynamic modeling of Gough–Stewart platform based on principle of virtual work. *Nonlinear Dynamics*, 2016, 83(4): 2393-2418.
[19] B Dasgupta, T S Mruthyunjaya. A Newton-Euler formulation for the inverse dynamics of the Stewart platform manipulator. *Mechanism and Machine Theory*, 1998, 33(8): 1135-1152.
[20] M Naser, A Alireza, D Jaspreet, et al. A comprehensive inverse dynamics problem of a stewart platform by means of Lagrangian formulation. *ASME 2017 Dynamic Systems and Control Conference*, Virginia, USA, 2017: 2017-5098.
[21] Y F Zhang, P Jin, J L Gong, et al. Dynamic modeling of viscous friction conditions of 3-RPS parallel robot. *Transactions of the Chinese Society of Agricultural Machinery*, 2018, 49(9): 374-381.
[22] J J You, C G Li, H T Wu. Research on Hamiltonian dynamics of parallel type six-axis accelerometer. *Journal of Mechanical Engineering*, 2012, 48(15): 9-17. (in Chinese)
[23] Y B Li, H Zheng, P Sun. Dynamic modeling and coupling analysis of 5-PSS/UPU parallel mechanism considering joint friction. *Journal of Mechanical Engineering*, 2019, 55(3): 43-52. (in Chinese)
[24] S W Fu, Y Yao, Y Q Wu. Comments on "A Newton–Euler formulation for the inverse dynamics of the Stewart platform manipulator". *Mechanism and Machine Theory*, 2007, 42(12): 1668-1671.
[25] S Pedrammehr, M Mahboubkhah, N Khani. Improved dynamic equations for the generally configured Stewart platform manipulator. *Mechanical Science and Technology*, 2012, 26(3): 711-721.
[26] X L Chen, W M Feng, Y S Zhao. Dynamic model of a 5-DOF parallel robot mechanism. *Transactions of the Chinese Society of Agricultural Machinery*, 2013, 44(1): 236-243.
[27] M C Geng, T S Zhao, C Wang, et al. Dynamic analysis of 4-UPS/UPR parallel mechanism. *Transactions of the Chinese Society of Agricultural Machinery*, 2014, 45(8): 299-306.
[28] Y G Li, Y M Song, Z Y Feng, et al. Inverse dynamics analysis of 3-RPS parallel mechanism based on Newton's Euler method. *Acta Aeronautica*, 2007, (5): 1210-1215.
[29] S Z Liu, Y Q Yu, G N Tong, et al. Kinematics and dynamics analysis of a 3 degrees of freedom parallel robot. *Journal of Mechanical Engineering*, 2009, 45(8): 11- 17. (in Chinese)
[30] H P Shen, J M Deng, K Wang. A two translation and one rotation parallel mechanism with zero coupling and positive solution of analytical position: China, 201961623865x. 2019-06-11.